Journal of Materials Chemistry C

A macromolecular assembly directed ceramic aerogel monolith material

Journal:	*Journal of Materials Chemistry C*
Manuscript ID	TC-ART-05-2020-002481.R1
Article Type:	Paper
Date Submitted by the Author:	13-Jun-2020
Complete List of Authors:	Yang, Ruizhe; University at Buffalo - The State University of New York Wang, Jieyu; University at Buffalo - The State University of New York An, Lu; University at Buffalo - The State University of New York Petit, Donald; University at Buffalo - The State University of New York Armstrong, Jason; University at Buffalo - The State University of New York Liu, Yuzi; Argonne national Laboratory, Center for Nanoscale Materials Huang, Yulong; University at Buffalo - The State University of New York, Mechanical & Aerospace Engineering Hu, Yong ; University at Buffalo - The State University of New York Shao, Zefan; University at Buffalo - The State University of New York Ren, Shenqiang; University at Buffalo - The State University of New York,

ARTICLE

A macromolecular assembly directed ceramic aerogel monolith material

Received 00th January 20xx,
Accepted 00th January 20xx

DOI: 10.1039/x0xx00000x

Ruizhe Yang[a,‖], Jieyu Wang[b,‖], Lu An[a], Donald Petit[a], Jason N. Armstrong[a], Yuzi Liu[c], Yulong Huang[a], Yong Hu[a], Zefan Shao[a], and Shenqiang Ren[a,b,d*]

Ceramic aerogel exhibits remarkable thermal insulation for energy efficiency, while it is indispensable to understand its nanoporous structure evolution to control its thermal regulation performance. In this study, we design and synthesize lightweight porous silica aerogel monolithic material, and demonstrate its thermal insulation performance regulated by the morphology of porous nanostructures controlled by surfactant induced self-assembly. The micelle networks and in-situ gas bubble formation guide the formation of uniform pores in the as-synthesized monolith, which shows a superior thermal and acoustic insulation and robust mechanical stability with a thermal conductivity of 0.032 W m^{-1} K^{-1}, a soundproof performance improvement by 17% at frequency of 800 Hz, and a 1.3 MPa compressive strength with Young's modulus of 15 MPa. The findings provide a new route to manufacture low-cost aerogel monolithic insulation materials for energy efficient building applications.

Introduction

Silica-based aerogel has ignited intense interest for many years due to its unique nanostructure. Specifically, it has high porosity, low density and large specific surface area at the same time.[1, 2] These characteristics give rise to its low thermal conductivity (5-100 mW/(mK)) and thus it is widely applied in thermal insulation materials.[2, 3] Its most representative porous structure is formed through a sol-gel process and the replacement of the liquid in gel pores by a gas ensures the stability of its network.[3-5] This process has been widely investigated by using different silica precursors (sodium silicate, tetramethyl orthosilicate, tetraethyl orthosilicate and methyltrimethoxysilane), hydrophobic solvents (alcohols with different lengths of carbon chain), and surface modification.[6-10] Surface modification is critical for the formation of aerogel during ambient pressure drying as the original hydrophilic aerogel would lose its durability during ambient pressure drying.[11] To overcome this challenge, organic solvents (e.g. TMCS/EtoH/n-hexane in a certain ratio) have been utilized to replace H in silanol group to reduce the shrinkage.[12] However, such process usually takes a long solvent exchange time for aerogel synthesis under ambient pressure.[13] Therefore, it is indispensable to look for alternatives for the synthesis and processing of ceramic aerogel materials.

The surfactant is the amphiphilic molecule that simultaneously exhibits both hydrophilic and hydrophobic characteristics, which could form the ordered nanostructures due to the occurrence of a pseudo 'self-assembly' process in the solution.[14, 15] This is a two-step process where surfactants firstly aggregate three-dimensionally to produce micelles at molecular level in a homogeneous solution.[16] When the critical micelle concentration is reached, these micelles continue to self-assemble in the nanoscale level. They aggregate and separate from the original solvent to give a new phase that named as 'supramolecular solvent' through a 'coacervation' phenomenon.[17-19] The supramolecular solvent is rich in surfactant molecules and can modify inorganic silica material components in the original homogeneous solvent due to the hydrophobic nature of the surfactant.[14] In other words, surfactant micelles use their hydrophobic side to 'support' silica network, which contributes to the less shrinkage and meanwhile maintains its porous structure induced low thermal conductivity. Here, we investigate the ambient pressure manufacturing of silica-based aerogel materials through the application of two ionic surfactants: cetrimonium bromide (CTAB) and sodium dodecyl sulfate (SDS) due to the ability of ionic strength in leading the self-assembly. The porous nanostructures of as-synthesized aerogel materials can be controlled by the concentration-dependent self-assembly of surfactant molecules, which play an important role in the thermal and acoustic insulation and mechanical strength of aerogel monolithic materials. The lightweight mechanically robust aerogel monolithic material shows a thermal conductivity as low as 0.032 W m^{-1} K^{-1}, a 17% reduction of noise at frequency of 800 Hz and a compressive strength of 1.3 MPa with Young's modulus of 15 MPa (Table 1). [20-24]

[a] *Department of Mechanical and Aerospace Engineering, University at Buffalo, The State University of New York, Buffalo, NY 14260, USA*
[b] *Department of Chemistry, University at Buffalo, The State University of New York, Buffalo, NY 14260, USA*
[c] *Center for Nanoscale Materials, Argonne National Laboratory, IL 60439*
[d] *Research and Education in Energy, Environment & Water (RENEW), University at Buffalo, The State University of New York, Buffalo, NY 14260, USA*
‖ Equal contribution.

Electronic Supplementary Information (ESI) available: The details on surfactant dependent thickness, surface area, pore width distribution and thermal conductivity, mechanical strength and soundproof performance at different frequencies. See DOI: 10.1039/x0xx00000x

Table 1. A comparison of thermal property and mechanical strength between this work and literature.

Silica Precursor	Surface treatment	Thermal conductivity (W/mK)	Testing Method	Young's Modulus (MPa)	Reference
TEOS	In-situ SDS	0.032	Home customized machine following the ASTM C518 standard measurement procedure	15	Our sample
TEOS	In-situ CTAB	0.036	Home customized machine following the ASTM C518 standard measurement procedure	/	Yang et al.
Vinyltriethoxysilane	Ethanol	0.037	A HotDisk TPS2500 thermal constant analyser based on the transient hot plane method	1.31	Yun et al.
TEOS	HMDZ	0.08	/	/	Guray et al.
TEOS	HMDZ/EtOH	0.09	C-T meter from Teleph company, France	/	Rao et al.

Materials and Methods

Ceramic Aerogel Preparation. First 3 mol L^{-1} g Urea (Sigma-Aldrich), 0.3 mol L^{-1} CTAB (Cetyltri76methylammonium bromide) or SDS (Sodium dodecyl sulfate), 1 mmol Acetic Acid was combined with 33 mL distilled water in a 100 ml beaker. This was stirred for 3 hours until the solution becomes transparent. Then 1.4 mol L^{-1} TEOS (Tetraethyl Orthosilicate) was added into the solution. This was then stirred for 10 minutes, which caused the solution to become semi-transparent. The solution was transferred to an aluminum vessel, the vessel was then tightly sealed. The oven was preheated to 60 °C for 1 hour, the vessel was then placed into the oven for 4 days. The samples (monolith and gel) were taken out from the vessel to a container filled with distilled water which was preheated to 60 °C. The samples were left in the container for two days. The water was changed several times during the process, which is done until the supernatant water was clear and all ammonia is removed. Then sample (gel) was stored in a sealed container for further application.

Properties Characterizations. The volume of the sample was measured through a pycnometer test which used helium gas to penetrate the aerogel sample. Specific surface area and the pore size distribution are analysed through a Brunauer-Emmett-Teller (BET) measurement, which was performed on a Tristar II 3020 (Micromeritics Corp. Atlanta, GA). Thermal conductivity was measured with a home customized machine following the ASTM C518 standard measurement procedure. A heat flux sensor that came from Fluxtaq company was calibrated with reference bulk polystyrene. Mechanical strength was measured through a uniaxial compressions test. It was performed on silica monoliths synthesized via CTAB and SDS surfactants by Mark-10 test stand. The constant load speed was 13 mm/min. The bulk dimensions were 1.8×1.8×1.6 cm^3. The compression tests would be stopped when the silica monolith failed. Acoustic insulation ability was tested in a home-designed sound box containing sound insulation reference material.

Results and Discussion

The schemes in Figure 1a and b show difference in the micelle structures of surfactant CTAB and SDS. In comparison, CTAB has a relatively longer hydrophobic carbon chain and smaller hydrophilic head, functional group.[25] Due to this unique structure, there is a limited repulsion between the heads resulting in the heads to assemble together during the self-assembly process which leaves the hydrophobic tail out surrounding the micelle structure (shown in Figure 1a).[14] This also results in a phase separation where there is a homogeneous precursors solution, however, the separation trend varies with the kind of surfactant used. For example, shown as Figure 1a, when CTAB is added into TEOS-water precursor, an opaque solid monolith is formed with a limited gel phase. The reason behind this phenomenon is that majority of CTAB micelles tend to separate from original solution and form a supramolecular phase, which then combines with silica nanoparticles in order to create a solid monolith. Minority of these micelles will be formed as tail to tail, leave hydrophilic sides outside and stay within the aqueous solution to create the gel phase. Besides, this accumulation of the solid monolith rises with increasing concentration of surfactant CTAB and reaches the optimum at 30 wt.% of CTAB (Figure S4). On the contrary, surfactant SDS is of a relatively larger functional group, hydrophilic head, and much shorter carbon chain, hydrophobic tail.[26] Therefore, there is much larger repulsion between the head groups so the SDS micelles will be likely to have the structure with hydrophobic tail inside and hydrophilic head outside, as shown in Figure 1b. Due to a completely opposite structure to CTAB micelle, the gel in water phase is much more attractive to SDS micelles, which means majority of them will tend to stay in the water phase. As a result, instead of solid monolith, more and more transparent gel in water phase will form with increasing concentration of surfactant SDS. Figure 1b shows the transformation and when 35 wt% SDS is added, the sample is transparent totally (see Figure S4). In addition, both kinds of micelles, before reaching their critical micelle concentration, will gradually become smaller and tighter with increasing concentration of surfactant CTAB and SDS. The whole porous structure also becomes more uniform due to smaller and more uniform packing of micelles. If the concentration is far larger than the critical concentration, the size of spherical micelle no longer changes, however, spherical micelles will aggregate into cylindrical ones and even hexagonal shape, as shown in Figure 1c.[16, 27, 28]

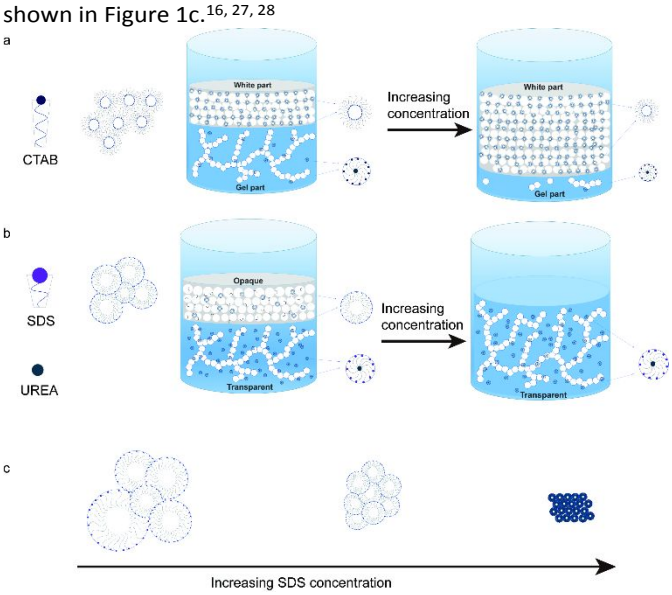

Fig.1 Schematic figure shows the opaque and transparent silica phase changing with increasing concentration of surfactant. a. For surfactant CTAB, the opaque silica phase dominant with

increasing concentration of CTAB. b. For surfactant SDS, the transparent silica phase preferable with increasing concentration of SDS. c. The morphology evolution of micelle with increasing the concentration of SDS. Spherical micelles becoming more organized and smaller and turning into cylindrical shapes when concentration increasing.

Both opaque silica monolith and transparent silica gel are further investigated, mainly focusing on the samples synthesized with the surfactant of SDS due to its scalable manufacturing nature (Growth of CTAB-based aerogel is shown in Figure S1, S2 and Table S1). Figure 2a shows the optical image of the transparent gel with light sky-blue colour. The detailed nanostructure of the dried gel can be readily observed from scanning electron microscopy (SEM) and transmission electron microscopy (TEM), where mesoporous silica nanostructures with pores are uniformly distributed and packed together with the average channel dimension of 10 nm. The SEM image of typical transparent gel (generated with 3.33 wt.% SDS is shown in Figure 2b and Figure S3, with 20 wt.% and 35 wt.% SDS are shown in Figure S3) exhibits a close pack structure with homogeneous pore structure distribution, where pore size is dependent on the reaction conditions, such as the concentration of surfactant, reaction temperature and time (which is discussed further in the following sections). The solid networks of transparent silica are constructed by nanoscale silica particles with micelle supramolecules formed by surfactant which are further characterized by TEM. As shown in Figure 2c, a large number of mesopores and micelles network channel in each particle are clearly observed due to the self-assembly effect of SDS micelles.

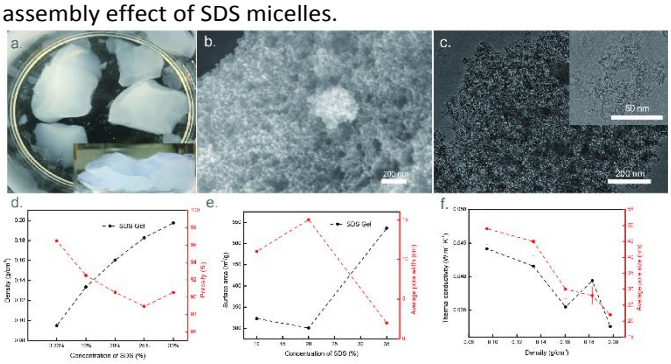

Fig.2 (a) Optical image of transparent aerogel. (b) SEM image of transparent aerogel from 3.33 wt.% SDS. (c) STEM image and the inserted figure show the micro structure of transparent aerogel from 20 wt.% SDS. (d) Gel part density and porosity changing with concentration of SDS. (e) Surface area and average pore size vs. concentration of SDS from 10 wt.% to 35 wt.%. (f) Thermal conductivity and average pore size vs. density of the transparent aerogel.

We further investigate material structure, surface area and thermal conductivity by tuning the concentration of surfactant SDS. With increasing concentration of SDS from 3.33 wt.%, 10 wt.%, 20 wt.%, 25 wt.% to 30 wt.%, the density of the transparent dried gel increases from 0.096 g/cm^3 to 0.20 g/cm^3, while the porosity decreases from 97.6% to around 90% in Figure 2d. With increasing SDS concentration, the micelles greatly strengthen the silica network, which cause the density increasement. BET measurements further look into the surface area changes of the gel phase with increasing concentration of SDS. At low concentration around 10 wt.% to 20 wt.%, the surface area sticks around 300-350 m^2/g with average pore width around 10-20 nm, shown in figure 2e (Pore width distributions for transparent gel prepared with 10 wt.%, 20 wt.% and 35 wt.% SDS are shown in Figure S4). However, when concentration of surfactant SDS reaches up to 35 wt.%, the surface area of transparent gel dramatically rises up to 550 m^2/g with average pore width around 2 nm. According to the phase diagram of SDS in water solution, when the concentration reaches 35 wt.%, surfactant SDS will change its morphology of nanostructure from spherical to hexagonal, leading to a jump of surface area of the transparent gel. Thermal resistance performance has also been tested. Figure 2f shows the thermal conductivity and average pore size of transparent gel decrease with increasing density. The increasement of SDS concentration causes the average pore size decrease from 50 nm to 20 nm, leading to a highly packed gel structure with a lower thermal conductivity dropping from 0.045 W m^{-1} K^{-1} to 0.032 W m^{-1} K^{-1} along. That's because thermal conductivity of aerogel mainly depends on gaseous voids and connectivity of the silica network.[29, 30] The increasing concentration of SDS micelles not only modifies the silica network, but also can work as a kind of 'polymer chain' due to its unique hydrophobic tail to support the silica network. Therefore, the degree of collapse of network decreases during the ambient pressure drying and the connectivity of the crosslinking structure can be maintained. Although porosity decreases a little, a great decrease in both average pore width and size when SDS concentration is increased to 35 wt.% greatly improves thermal insulation performance.

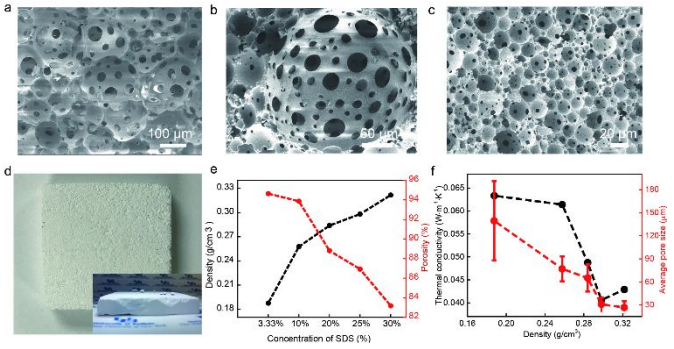

Fig.3 SEM images of solid monoliths from the SDS concentration of (a) 3.33 wt.% (b) 10 wt.% and (c) 20 wt.% at, respectively, showing structure of monoliths transformation change from open pore to close pore. (d) Optical image of monolith of 3.33 wt.% SDS. The scale bar is 12 mm. Inset image shows hydrophobicity of the sample. (e) Density and porosity change with concentration of SDS. (f) Thermal conductivity and density, average pore size relationship.

Due to phase separation of organic SDS surfactants in aqueous solution, the opaque bulk phase is self-assembled above the wet transparent gel in one same pot. The microstructure of the bulk monoliths would contribute the thermal/acoustic insulation and mechanical performance. The detailed nanostructure of the opaque solid monolith can be readily observed from SEM where the nanostructures with the pores are uniformly distributed and packed together consisting of mesoporous silica nanoparticle. Figures 3a-3c show SEM images of pore structure in typical opaque solid monolith with increasing concentration of surfactant from 3.33 wt.% to 10 wt.% and 20 wt.%, which also shows a close packed structure

with homogeneous pore size distribution. Furthermore, with increasing concentration of SDS, each micelle molecule becomes smaller and more uniform, which leads to a pore structure transformation from an open pore structure to close pore structure. Figure 3d shows a typical optical image of opaque solid monolith. Also, we further investigate material characterization and performance with density surface area and thermal conductivity by tuning the concentration of surfactant SDS. Increasing concentration of SDS from 3.33 wt.%, 10 wt.%, 20 wt.%, 25 wt.% to 30 wt.%, density of the opaque solid monolith shows an increasing tendency, from 0.18 g/cm^3 to 0.32 g/cm^3, while porosity shows an opposite decreasing tendency from 94% to 83%, which is matched with the density change, shown in Figure 3e. Figure 3f shows the change of thermal conductivity of monolith with the change of density. When the concentration of SDS is increased to 25 wt.%, the density is 0.30 g/cm^3 and thermal conductivity is reduced to 0.041 W m^{-1} K^{-1}. When doing a comparison between transparent and opaque solid silica monolith, it suggests that, from the aspects of density, porosity, average pore size and thermal conductivity, transparent silica shows a pronounced performance. That's firstly due to the hydrophilicity of surfactant SDS, which leads it to be more attractive to water and thus majority of SDS micelles aggregate in water, rather than the monolith part and then its hydrophobicity well modifies the silanol groups in the transparent part.

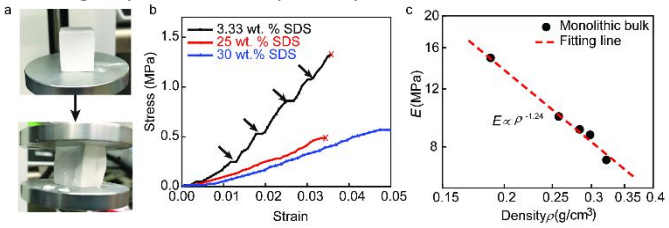

Fig.4 (a) The demonstration of uniaxial compression on the monoliths of 3.33 wt% SDS. (b) Stress-strain curves of monoliths with different concentrations of SDS showing high mechanical strength. Mechanical strength becomes lower with increasing concentration of SDS. (c) Young's modulus *E* decreasing with increasing density *ρ* due to increasing concentration of SDS.

The microstructure of bulk monolith caused by phase separation of organic SDS surfactants in aqueous solution plays the important role in the mechanical performance of the monolith. The uniaxial compression tests are performed to explore the effect of SDS concentration on the mechanical properties of opaque solid monolith (the effect of CTAB has also been tested and results are shown in Figure S8 and S9). Due to the brittle ceramic nature, the compression is stopped once apparent surface cracks or surface delamination appears on the aerogel bulk (see the optical images of 3.33% SDS sample before and after compression in Figure 4a).[31] The stress-strain curves of 3.33 wt.%, 25 wt.% and 30 wt.% concentration of SDS templated samples are shown in Figure 4b, where the red cross indicating the apparent surface failure. With increasing SDS concentration, the slopes of the stress-strain curves are decreasing which indicates the decreasing rigidity of samples. That's because surfactants prefer to aggregate in the gel part of more SDS-concentrated samples, where the silica network is more hydrophobic and stronger after drying and thus, the corresponding solid part is weak due to the lack of surfactant modification. And when SDS concentration reaches over 35 wt.%, all solution turned into gel part without any monolithic bulk, then the dried gel powders cannot be measured by compression here. For 3.33 wt.% SDS sample, there are multiple strain bursts in the stress-strain curve before reaching the plateau, which are due to the micro-cracks between pores inside the bulk. After the strain reaches ~0.033, the stress becomes the plateau, indicating the apparent surface cracks or surface delamination happens. Here, this maximum stress (1.3 MPa) is regarded as the strength of the monolith bulk, which is much stronger than aerogels in other works, such as silica fibrous aerogel with 10 KPa strength.[32] When the SDS concentration increases beyond 25 wt.%, the samples become much more brittle compared with that of 3.33 wt.% SDS sample. Also, there is no apparent strain burst, which means that the higher SDS concentration could hinder the microcrack initiation inside the bulk. For 25 wt.% SDS, the maximum strain before the apparent surface cracks or delamination is roughly same as that of 3.33 wt.% SDS sample. This probably indicates that SDS concentration< 25 wt.% affects the rigidity but not the brittle nature. However, when SDS concentration reach 30 wt.%, the stress-strain curve becomes smoother and the maximum strain could reach ~5%, which indicates the sample becomes more ductile. Also, the compression curves of monoliths in this study is different from that of some literatures which containing the stages of linear elastic, elastic-plastic (or collapse), and densification.[33, 34] This may arise from the hierarchical micro-pore structure changes in Figure 3c. When the concentration reaches 30%, the pore structure changes from open pore to closed pore, which leads to a certain plastic deformation without the suddenly surface delamination. The Young's modulus *E* of the solid monolith vs. density ρ are plotted in Figure 4c. The *ρ* of monolith tends to increase with the increasing concentration of SDS, however, *E* decreases from 15 MPa to 4 MPa with the increasing *ρ* (in other words, with the increasing SDS percent), which represents the lower in stiffness and matches the result shown in Figure 4b. The fitting line from the data in Figure 4c shows the power law relationship between *E* and *ρ* of monolith samples as $E \propto \rho^n$, where n is -1.24 in this study. This n value is different from the power-law scaling value from 1 to 3.8 in the literatures which are dominated by the ideal stretching or the bending mechanism.[35, 36] The negative power law scaling in this study is resulted from SDS phase separation, pore structures changes, and the interparticle bonding between silica nanoparticles. The volume ratio between bulk monolith and gel part by SDS surfactants phase separation in aqueous decreases with increasing SDS concentration, where the interparticle bonding between silica nanoparticles in monolith is larger than the bonding between nanoparticles in gel. This is the reason for the rigid and strong bulk monolith (e.g., 1.3 MPa strength for monolith of 3.33 wt.% SDS with E = 15 MPa) compared with that of the loosely aerogel powders dried from gel. The interparticle bonding among monoliths becomes weak with increasing SDS concentration until 35 wt.%, and afterwards, the interparticle bonding is weak enough to diminish the opaque bulk into all gel for 35 wt.% SDS. This decreasing interparticle bonding in bulk monolith result in the decreasing E, while the microstructures of pore morphology change the monoliths' density. With increasing SDS concentration, the microstructure of monolith changes from open pore structure to closed pore structure with the decreased average pore structure size from ~180 μm to ~30 μm in Figure 3f. Since the pore structure becomes smaller, the porosity

becomes lower, which causes the bigger density. Therefore, our monolith bulks demonstrate a different power-law scaling relationship in Figure 4c.

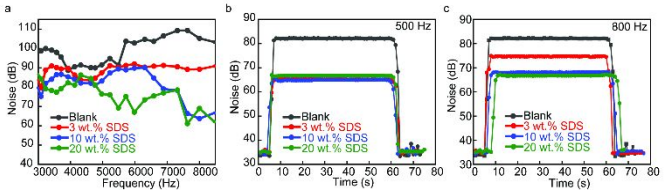

Fig.5 Soundproof performance of monoliths (6 mm) by different concentrations of SDS under (a) high sound frequency from 3,000 Hz to 8,500 Hz, (b) sound frequency of 500 Hz, (c) sound frequency of 800 Hz.

Solid monolith synthesized with surfactant SDS also performs well in acoustic insulation under both low and high frequency conditions because of the network of silica aerogel and high porosity maintained by the surfactant assembly. As shown in Figure 5a, the aerogel monolith reduces the noise across the frequency range from 3,000 to 8,000 Hz, suggesting a higher concentration of SDS for better soundproof performance (Soundproof tests under 1,000, 2,000 and 3,000 Hz are shown in Figure S10). In a soundproof test under a frequency of 500 Hz, opaque aerogels generated at different concentration of SDS (3 wt.%, 10 wt.% and 20 wt.%) show similar performance (Figure 5b). However, when the test frequency is increased to 800 Hz (Figure 5c), the difference is much pronounced and the specimen synthesized with high concentrated (20 wt.%) of surfactant show a pronounced soundproof performance and the noised is reduced to 17%. Change of density of silica monolith is related to the increase concentration of SDS. Shown as Figure 3e and 3f, with the increase of SDS concentration, density increases and average pore size decreases, which contributes to the increase of airflow resistivity and coefficient of sound absorption and therefore, leading to an improved soundproof performance.[37] In addition, without SDS modification, silica monolith would be hydrophilic and the network prefers to absorb water in the air, which would then be trapped in its pores and decreases the quantity of acoustic insulation.[38] In other words, the increase of SDS concentration contributes to hydrophobicity and thus ensures the performance of soundproofing.

Conclusions

In summary, we demonstrate lightweight silica aerogel that synthesized in in-situ surfactant reaction with a high porosity, small pore size and outstanding thermal and acoustic insulation performance. Surfactants can self-assemble into micelles, which modifies the silica network with their hydrophobic sides, giving great strengths to the mesoporous structure of aerogel. Due to opposing micelle structure, with the increase of surfactant concentration, aerogel generated with CTAB tends to be mostly solid white monolith while aerogel made from SDS are composed mostly of transparent gel. We mainly focus on both transparent and opaque part of samples synthesized with SDS. With the increasing concentration of SDS, thermal conductivity of the gel goes down to 0.032 W m^{-1} K^{-1}. For the white monolith, sample generated with lower concentration of SDS shows better mechanical strength while that generated with higher SDS concentration does better in noise reduction. Sample prepared with 3.33 wt.% SDS shows a 1.3 MPa compressive strength with Young's modulus of 15 MPa and that prepared with 20 wt.% SDS can reduce 17% noise. The generation of surfactant-induced suggests that replacement of traditional organic surface modification by in-situ surfactant reaction is feasible and the product can be widely applied in thermal insulation materials with strong mechanical property and remarkable noise-reduction ability.

Conflicts of interest

The authors declare no competing financial interest.

Corresponding author

shenren@buffalo.edu

Acknowledgements

R. Yang and J. Wang are equal contribution. This work at University at Buffalo is supported by the U.S. Department of Energy's Office of Energy Efficiency and Renewable Energy (EERE) under the Building Technology Office (BTO) Award Number DE-EE0008675. This work was performed, in part, at the Center for Nanoscale Materials, a U.S. Department of Energy Office of Science User Facility, and supported by the U.S. Department of Energy, Office of Science, under Contract No. DE-AC02-06CH11357.

Notes and references

1. J. P. Vareda, P. Maximiano, L. P. Cunha, A. F. Ferreira, P. N. Simões and L. Durães, *Journal of colloid and interface science*, 2018, **512**, 64-76.
2. H. Maleki, L. Durães and A. Portugal, *Journal of Non-Crystalline Solids*, 2014, **385**, 55-74.
3. T. Linhares, M. T. P. de Amorim and L. Durães, *Journal of Materials Chemistry A*, 2019, **7**, 22768-22802.
4. J. P. Randall, M. A. B. Meador and S. C. Jana, *ACS applied materials & interfaces*, 2011, **3**, 613-626.
5. A.-M. Siouffi, *Journal of Chromatography A*, 2003, **1000**, 801-818.
6. A. A. Pisal and A. V. Rao, *Journal of Porous Materials*, 2016, **23**, 1547-1556.
7. A. V. Rao, S. D. Bhagat, H. Hirashima and G. Pajonk, *Journal of colloid and interface science*, 2006, **300**, 279-285.
8. F. He, H. Zhao, X. Qu, C. Zhang and W. Qiu, *journal of materials processing technology*, 2009, **209**, 1621-1626.
9. A. Hilonga, J.-K. Kim, P. B. Sarawade and H. T. Kim, *Journal of Alloys and Compounds*, 2009, **487**, 744-750.
10. S.-W. Hwang, T.-Y. Kim and S.-H. Hyun, *Journal of colloid and interface science*, 2008, **322**, 224-230.
11. A. P. Rao and A. V. Rao, *Journal of non-crystalline solids*, 2008, **354**, 10-18.
12. G. Wu, Y. Yu, X. Cheng and Y. Zhang, *Materials Chemistry and Physics*, 2011, **129**, 308-314.
13. A. P. Rao, A. V. Rao and G. Pajonk, *Applied surface science*, 2007, **253**, 6032-6040.
14. A. Ballesteros-Gómez, M. D. Sicilia and S. Rubio, *Analytica Chimica Acta*, 2010, **677**, 108-130.
15. D. Philp and J. F. Stoddart, *Angewandte Chemie International Edition in English*, 1996, **35**, 1154-1196.
16. D. F. Evans and H. Wennerström, 1999.
17. A. Ballesteros-Gómez, S. Rubio and D. Pérez-Bendito, *Journal of Chromatography A*, 2009, **1216**, 530-539.

18. M. Cantero, S. Rubio and D. Pérez-Bendito, *Journal of Chromatography A*, 2004, **1046**, 147-153.
19. I. Casero, D. Sicilia, S. Rubio and D. Perez-Bendito, *Analytical Chemistry*, 1999, **71**, 4519-4526.
20. R. Yang, F. Hu, L. An, J. N. Armstrong, Y. Hu, C. Li, Y. Huang and S. Ren, *Nano Letters*, 2019.
21. S. Yun, H. Luo and Y. Gao, *Journal of Materials Chemistry A*, 2015, **3**, 3390-3398.
22. J. L. Gurav, A. V. Rao and D. Y. Nadargi, *Journal of sol-gel science and technology*, 2009, **50**, 275-280.
23. A. P. Rao, G. Pajonk and A. V. Rao, *Journal of materials science*, 2005, **40**, 3481-3489.
24. S. He and X. Chen, *Journal of Non-Crystalline Solids*, 2017, **463**, 6-11.
25. M. Cano-Sarabia, A. Angelova, N. Ventosa, S. Lesieur and J. Veciana, *Journal of colloid and interface science*, 2010, **350**, 10-15.
26. M. Bergström and J. S. Pedersen, *Physical Chemistry Chemical Physics*, 1999, **1**, 4437-4446.
27. W. Li, M. Zhang, J. Zhang and Y. Han, *Frontiers of Chemistry in China*, 2006, **1**, 438-442.
28. A. W. Dong, C. Fong, A. J. Hill, B. J. Boyd and C. J. Drummond, *Journal of colloid and interface science*, 2013, **402**, 173-179.
29. L. Durães, H. Maleki, J. P. Vareda, A. Lamy-Mendes and A. Portugal, *MRS Advances*, 2017, **2**, 3511-3519.
30. F. Hu, S. Wu and Y. Sun, *Advanced Materials*, 2019, **31**, 1801001.
31. L. An, D. Zhang, L. Zhang and G. Feng, *Nanoscale*, 2019, **11**, 9563-9573.
32. L. Dou, X. Zhang, X. Cheng, Z. Ma, X. Wang, Y. Si, J. Yu and B. Ding, *ACS applied materials & interfaces*, 2019, **11**, 29056-29064.
33. F. Jiang, S. Cui, C. Rungnim, N. Song, L. Shi and P. Ding, *Chemistry of Materials*, 2019, **31**, 7686-7695.
34. X. Zeng, L. Ye, S. Yu, R. Sun, J. Xu and C.-P. Wong, *Chemistry of Materials*, 2015, **27**, 5849-5855.
35. H. Kashani, Y. Ito, J. Han, P. Liu and M. Chen, *Science advances*, 2019, **5**, eaat6951.
36. L. R. Meza, S. Das and J. R. Greer, *Science*, 2014, **345**, 1322-1326.
37. L. Cao, Y. Si, Y. Wu, X. Wang, J. Yu and B. Ding, *Nanoscale*, 2019, **11**, 2289-2298.
38. F. D'Alessandro, G. Baldinelli, F. Bianchi, S. Sambuco and A. Rufini, *Construction and Building Materials*, 2018, **158**, 264-274.

TOC

A macromolecular assembly induced transparent and opaque ceramic aerogel material